Tomographic Surface X-ray Diffraction

HANNA SJÖ
DEPARTMENT OF PHYSICS | FACULTY OF SCIENCE | LUND UNIVERSITY

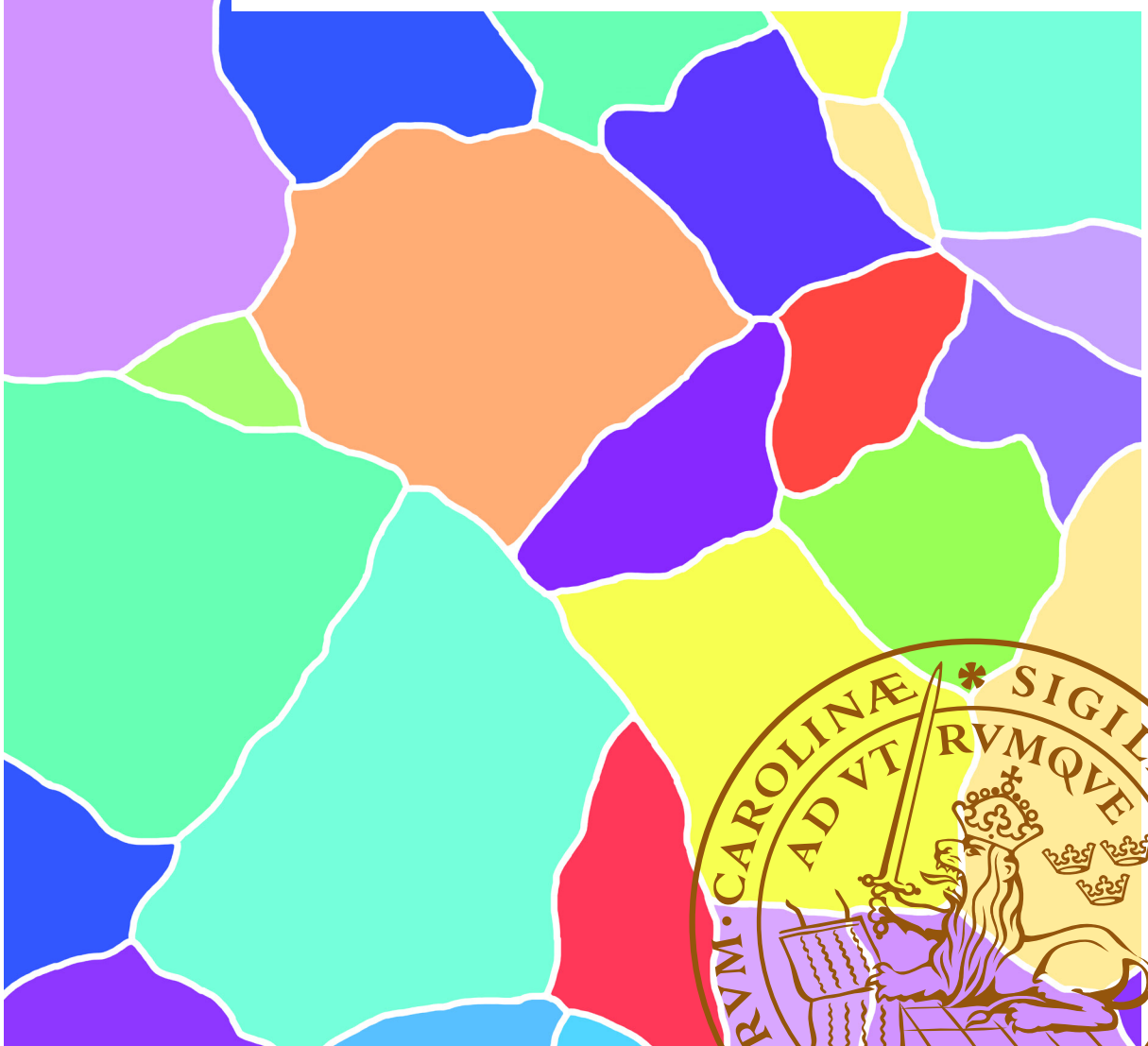

Printed by Media-Tryck, Lund 2025 NORDIC SWAN ECOLABEL 3041 0903

ISBN 978-91-8104-515-4
Division of Synchrotron Radiation Research
Department of Physics
Faculty of Science
Lund University

Tomographic Surface X-ray Diffraction

Tomographic Surface X-ray Diffraction

by Hanna Sjö

LUND
UNIVERSITY

Thesis for the degree of Licentiate
Thesis advisors: Johan Gustafson, Jesper Wallentin
Faculty opponent: Uta Hejral

To be presented, with the permission of the Faculty of Science of Lund University, for public criticism in lecture hall K457 at the Department of Physics on Tuesday, the 27th of May 2025 at 13:15.

Organization
LUND UNIVERSITY

Department of Physics
Box 118
SE–221 00 LUND
Sweden

Document name
LICENTIATE THESIS

Date of defence
2025-05-27

Sponsoring organization

Author(s)
Hanna Sjö

Title and subtitle
Tomographic Surface X-ray Diffraction

Abstract
The atomic structure of catalytic surfaces and its relation to function is important for the understanding and development of industrial catalysts. However, many surface sensitive methods are limited to low-pressure environments, creating a gap between experimental results and reality, and it is not certain that the findings can be applied to the real system. Surface X-ray diffraction is a method that is not limited to low pressures but is, on the other hand, limited to single crystals. This limitation is due to the long beam footprint caused by the grazing incidence angle needed to achieve surface sensitivity. In this thesis, we present the development of *tomographic surface X-ray diffraction,* an approach that enables surface X-ray diffraction measurements of polycrystalline surfaces. The tomographic surface X-ray diffraction approach can be divided into two steps: grain mapping using grazing incidence X-ray diffraction and sorting of surface X-ray diffraction signal from a polycrystalline sample.

The grain mapping, introduced in Paper I, uses Bragg reflections to determine grain orientation, and generate spatial maps of the grains across the sample surface. The result is maps comparable to maps from electron backscatter diffraction and the approach can distinguish grains as small as the beam width.

The signal-sorting step utilizes the grain map to assign surface diffraction signals to individual grains. At a given angle, the same signal should be present at all translations with the beam over a single grain and not be present outside the grain boundaries. By comparing the spatial occurrence of each signal with the grain map, single crystal diffraction patterns can be extracted from the measurements of the polycrystalline sample. This can then be applied to industry-relevant systems to study many surface orientations simultaneously.

Key words
surface x-ray diffraction polycrystalline, palladium

Classification system and/or index terms (if any)

Supplementary bibliographical information

Language
English

ISSN and key title

ISBN
978-91-8104-515-4 (print)
978-91-8104-516-1 (pdf)

Recipient's notes

Number of pages
78

Price

Security classification

Signature _____ Date 2025-04-09

Tomographic Surface X-ray Diffraction

by Hanna Sjö

LUND
UNIVERSITY

Cover illustration front: An illustration of grains from a polycrystalline surface. The drawing is loosely based on the EBSD map from Paper I.

Funding information: The thesis work was financially supported by the Swedish Research Council (project number 2021-05846).

Faculty of Science, Department of Physics

ISBN: 978-91-8104-515-4 (print)
ISBN: 978-91-8104-516-1 (pdf)

Printed in Sweden by Media-Tryck, Lund University, Lund 2025

Contents

List of publications

I **Surface grain orientation mapping using grazing incidence X-ray diffraction**
Hanna Sjö, A. Shabalin, U. Lienert, J. Hektor, A. Schaefer, P.-A. Carlsson, C. Alwmark, J. Gustafson
Surface Science (2025) 754, 122693

II **Tomographic surface X-ray diffraction - A method for studying polycrystalline surfaces**
Hanna Sjö, J. Gustafson
In manuscript

Abstract

The atomic structure of catalytic surfaces and its relation to function is important for the understanding and development of industrial catalysts. However, many surface sensitive methods are limited to low-pressure environments, creating a gap between experimental results and reality, and it is not certain that the findings can be applied to the real system. Surface X-ray diffraction is a method that is not limited to low pressures but is, on the other hand, limited to single crystals. This limitation is due to the long beam footprint caused by the grazing incidence angle needed to achieve surface sensitivity. In this thesis, we present the development of *tomographic surface X-ray diffraction,* an approach that enables surface X-ray diffraction measurements of polycrystalline surfaces. The tomographic surface X-ray diffraction approach can be divided into two steps: grain mapping using grazing incidence X-ray diffraction and sorting of surface X-ray diffraction signal from a polycrystalline sample.

The grain mapping, introduced in Paper I, uses Bragg reflections to determine grain orientation, and generate spatial maps of the grains across the sample surface. The result is maps comparable to maps from electron backscatter diffraction and the approach can distinguish grains as small as the beam width.

The signal-sorting step utilizes the grain map to assign surface diffraction signals to individual grains. At a given angle, the same signal should be present at all translations with the beam over a single grain and not be present outside the grain boundaries. By comparing the spatial occurrence of each signal with the grain map, single crystal diffraction patterns can be extracted from the measurements of the polycrystalline sample. This can then be applied to industry-relevant systems to study many surface orientations simultaneously.

Popular summary in English

Much of modern industry, relies on chemical reactions that take place on the surface of solid materials. These surfaces are where the solid comes into contact with a surrounding gas or liquid. The speed and efficiency of these reactions depend on the environment, such as pressure and temperature. Different conditions not only influence the reaction itself but also affect the surface of the material. These changes occur at the atomic level, with atoms rearranging on the surface.

To put that in perspective, the distance between atoms is tiny, much smaller compared to us than our size compared to the Earth. This makes it a considerable challenge to obtain detailed information about the structure and changes on a material's surface, especially when trying to replicate the conditions experienced inside a factory or an engine.

One important aspect that influences surface behavior is how the atomic lattice is "cut" to form the surface. Metals naturally form grids of atoms, often in the form of an enormous series of cubes with atoms at the corners and sometimes within the cube itself. When this three-dimensional stack of cubes ends to form a surface, the cut does not necessarily follow the side of the cube. Instead, it can occur at any angle. As a result, the atoms exposed to the outside world will be arranged differently depending on the angle of the cut. This is known as *surface orientation*.

In real materials, many of these surface orientations exist at the same time. Typically when studying the surfaces, different orientations are measured one by one. However, this process becomes very time-consuming since there are many possible orientations. If the different orientations influence the reaction in distinct ways, it may also be important to study them together in order to understand their combined effect.

In this thesis, we use a technique called surface X-ray diffraction, which allows us to measure how atoms are arranged on a surface. One major advantage of this method is that it can operate under realistic conditions, such as high pressure, which is uncommon for surface-sensitive techniques. However, conventional surface X-ray diffraction can only be applied to samples with a single surface orientation. To address this limitation, we introduce a development of the method called *tomographic surface X-ray diffraction*. This approach enables the measurement of surfaces with multiple orientations simultaneously while maintaining the advantages of the original technique.

Populärvetenskaplig sammanfattning på svenska

Stora delar av vår moderna industri är beroende av kemiska reaktioner som sker på ytan av metaller då det är här metallen kommer i kontakt med en omgivande gas eller vätska. Hastigheten och effektiviteten av dessa reaktioner beror på miljön den befinner sig i, såsom tryck och temperatur. Olika förhållanden påverkar inte bara själva reaktionen utan även materialets yta. Att förstå hur förändringarna på ytan hänger ihop med de önskade reaktionerna och vice versa är något som ofta studeras i ytfysik. Förändringarna som åsyftas här sker på atomnivå, med atomer som ändrar sin ordning på ytan.

För att sätta det i perspektiv är avståndet mellan atomerna mycket litet, mycket mindre jämfört med en människa än skillnaden på en människa och jorden. Detta gör att det är en stor utmaning att få detaljerad information om strukturen och förändringarna på ett materials yta, särskilt när man försöker återskapa de förhållanden materialet utsätts för i en fabrik eller motor.

En viktig aspekt som påverkar ytbeteendet är hur metallen skärs när ytan skapas. Metaller bildar naturligt nät av atomer, ofta i form av en serie kuber med atomer i hörnen och ibland inne i själva kuben. När detta tredimensionella nät av kuber slutar för att skapa en yta, följer inte snittet nödvändigtvis sidan av kuben. Istället kan slutet ske i vilken vinkel som helst. Som ett resultat kommer atomerna som exponeras för omvärlden att ha olika strukturer beroende på snittets vinkel. Detta kallas för *ytorientering*.

I de metaller som används i viktiga reaktioner finns många av dessa ytorienteringar samtidigt. Inom ytforskning mäts ofta varje ytorientering en efter en, men eftersom det finns många möjliga orienteringar blir denna process mycket tidskrävande. Om de olika orienteringarna påverkar reaktionen på olika sätt kan det vara viktigt att studera dem tillsammans för att förstå deras kombinerade effekt.

I detta arbete använder vi en teknik som kallas ytröntgendiffraktion, som gör att vi kan mäta hur atomer är ordnade på en yta. En stor fördel med denna metod är att den fungerar under realistiska förhållanden, såsom höga tryck, vilket är ovanligt för ytkänsliga tekniker. Konventionell ytröntgendiffraktion kan dock endast tillämpas på prover med en enda ytorientering. För att komma förbi denna begränsning presenteras här en utveckling av ytröntgendiffraktion som kallas *tomografisk ytröntgendiffraktion*. Med denna utveckling möjliggörs mätningar av ytor med flera orienteringar parallellt, samtidigt som fördelarna med den ursprungliga tekniken bibehålls.

Acknowledgements

There are many people who deserve gratitude for their contributions to this project and to my time as a PhD student so far, but I will keep this short.

First and foremost, I want to thank my supervisor, **Johan Gustafson**, who has been the main support throughout this project and the writing of this thesis. Your encouragement and optimism have been vital to my development, and I look forward to two more years of working together. I am also grateful to my co-supervisor, **Jesper Wallentin**, who has been an additional source of support whenever needed.

Much of this work has relied on excellent support, both during and after experiments. **Andreas Schaefer**, **Johan Hektor**, and **Per-Anders Carlsson** have all been invaluable, not only during beamtimes but also in the development of TSXRD. I also want to acknowledge the essential support from the team at P21.2. I would not have made it this far in developing the analysis without the foundational work by **Anatoly Shabalin**; I am truly grateful that you trusted me to finalize what you started. **Ulrich Lienert** has offered constant support at every beamtime, always bringing insightful ideas and deep expertise. No beamtime would have run as smoothly without the outstanding experimental support from **Zoltan Hegedüs**. Thanks also to **Carl Alwmark** for all the help with the EBSD measurements.

Thanks to **Patrik**, **Anne**, and **Josefine** for everything you do to keep the wheels of the division turning. Many others at **Sljus** also deserve mention for scientific support, collaboration, and for making every day at the division full of laughter and joy. Since I still have a few more years with you, I'll save your full acknowledgment for later.

This work would not have been possible without my wonderful **friends** outside the division, who I've had the pleasure of spending time with during my many years in Lund. I also have an incredible **family** who has supported me every step of the way. And finally, **Gustav**, your unwavering support means everything—I couldn't imagine a better partner to share this journey with.

List of abbreviations

2D	two-dimensional
3D	three-dimensional
3DXRD	three-dimensional X-ray diffraction
BCC	body-centered cubic
COM	center of mass
CT	computed tomography
CTR	crystal truncation rod
DCT	diffraction contrast tomography
EBSD	electron backscatter diffraction
EMFP	elastic mean free path
FCC	face-centered cubic
FIB	focused ion beam
HCP	close-packed hexagonal
HESXRD	high energy surface X-ray diffraction
IPF	inverse pole figure
SC	simple cubic
SDD	sample detector distance
SEM	scanning electron microscope
SSR	superstructure rod
SXRD	surface X-ray diffraction
TSXRD	tomographic surface X-ray diffraction
XRD	X-ray diffraction

Tomographic Surface X-ray Diffraction

Introduction

Chemical reactions using catalysts are not only important but absolutely necessary for our life on Earth. Without the catalysts cleaning the engine exhaust, cities full of with cars would be filled with toxic gases, and without the Haber–Bosch process that turns nitrogen from the atmosphere into fertilizer, we would not be able to feed the world's population. With growing needs from society, a growing climate crisis, and certain key catalytic materials becoming more rare and expensive, the development of new catalysts is an active and critical area of research[1]. In this development, there is a need to understand the well-used catalytic materials and the potential limitations of the materials that are not currently used.

Catalysis can be categorized in a few different ways. There is homogeneous catalysis, where both reactants and catalyst have the same phase, and heterogeneous catalysis, where the catalyst and reactants have different phases. Typically in the latter case, the catalyst is a solid in a liquid or a gas. Focusing on heterogeneous catalysis, the interface between reactants and the catalytic material plays a crucial role. Since this will be the catalyst surface, we aim to understand surface processes down to the atomic rearrangements occurring during reactions. Finding structure-functionality relations can help us to understand the catalyst.

Industrial catalysts are often nano-particles on some support material. Since the surfaces of nano-particles are very challenging to study, surface scientists often resort to simple model samples with one well-defined surface. The nanoparticles will have many facets, a high surface-to-bulk ratio, and attachment to the support, all of which can affect the reactions. It is not certain that the properties of the simplified model sample can be applied to the real catalyst, and this discrepancy is known as the *material gap*. In this work, we focus on polycrystalline surfaces, which are surfaces with grains of various crystalline orientations. Our polycrystalline surfaces are flat, polished surfaces with various orientations and grain sizes. Polycrystalline samples still have a gap towards real

catalysts, but they can provide information about more than one facet at a time, measure different facets under the same conditions, and have grain boundaries and potential synergistic effects between different grains. Although it does not completely close the gap, it does provide a more realistic model system.

Not only is there a need to understand more details about surface systems, but also to get these details under more realistic conditions. Many techniques that can provide detailed surface information are very limited when it comes to pressure, often since they are electron-based and the electron has a very limited mean free path. This leaves two options. One is to measure at a lower pressure, which is very similar to measuring a simplified sample in that it is uncertain if the information applies to the real system, which results in what is known as the *pressure gap*. Alternatively, the system can be studied after it has been separated from the reaction environment. The latter would entail looking at the surface after some reaction, also known as *ex situ*. The surfaces during reactions are dynamic systems, and there can be many intermediate states during the reaction, which an *ex situ*-approach then will not be able to study. We thus want a method that can provide detailed surface information during the reaction, or *in situ*. When we also include that the measurements are performed on a system close to industrial conditions, we have *operando* measurements.

There is a wide selection of techniques for surface studies, all with different advantages and limitations. The basic technique used in this work is surface X-ray diffraction (SXRD), which can be used in high gas pressures and liquid environments without the same limitations as electron-based techniques. It is very surface sensitive but lacks spatial resolution over the surface, and has therefore mainly been used for simple model samples. To overcome this limitation, we are developing a new method called tomographic surface X-ray diffraction (TSXRD). The new method is presented in two parts, where the surface mapping needed for the surface analysis is presented in Paper **I**, and the surface structure analysis is presented in Paper **II**. These parts include both the development of the measurement procedure and the subsequent data analysis.

In this introduction, the work has been motivated by the importance of *operando* measurements, while the results presented in Paper **I** and Paper **II** are all from *ex situ* measurements. The work presented has a focus on the method development, with a simple sample and simple changes to the surface as a proof of concept for a method that can later be applied to a more complex system.

Outline

In this thesis, I will first cover basic crystallography, which is necessary to understand descriptions of polycrystalline surfaces and diffraction results. I will emphasize the crystalline structure of palladium since this is the material used in the work presented here.

This thesis focuses on SXRD, so there is a more detailed description of diffraction theory. The method development has taken advantage of some three-dimensional X-ray diffraction (3DXRD) methods. Because there are similarities between what 3DXRD does in three dimensions and what we have done on a surface, there is a more detailed description of some algorithms used. To get reference maps in the development of grain mapping using diffraction, electron backscatter diffraction (EBSD) has been used. It is not vital to understand EBSD in detail, but a summary of EBSD theory is provided.

The final chapter briefly describes the measurement procedure and analysis approach in TSXRD. While the descriptions in Paper **I** and **II** are more technical, this chapter aims to give a more general description of the method together with a short outlook of the near future for TSXRD.

Crystalline structures

Many materials, including most metals, have a crystalline structure. The structure impacts many of the material's properties. Here, some forms of describing crystalline structures and surfaces are presented together with some of the properties of different surfaces.

Basics of the crystalline lattice

A crystal will be built up of repeating building blocks where the periodicity can be described using the Bravais lattice. Any two lattice points have exactly the same surrounding and can be joined by a lattice vector using

$$\mathbf{R} = m_1\mathbf{a}_1 + m_2\mathbf{a}_2 + m_3\mathbf{a}_3, \tag{1}$$

where $\mathbf{a}_i$ are basis vectors and m_i are integers. The volume spanned by the basis vectors is called the unit cell. Inside the unit cell, one or more atoms are placed at specific positions and the repetition of the unit cell at each lattice point builds up the whole crystalline structure. The unit cell, and hence the basis vectors, of a specific crystal structure can be chosen in several different ways. The alternative with the smallest volume is called the primitive unit cell.

It is very common to work with a cubic unit cell. The simplest of the cubic structures is the simple cubic (SC) structure, where the primitive unit cell is cubic. However, in metals, the most common structures are face-centered cubic (FCC), body-centered cubic (BCC), and close-packed hexagonal (HCP), out of which the first two are also described using a cubic unit cell. SC, FCC and BCC are shown in Figure 1. Both FCC and BCC can be described with a smaller unit cell than the one shown in the figure, but the cubic description is often the most convenient. Since the work included in this thesis involves measurements of Pd, which has an FCC structure, the FCC lattice will henceforth be used in most examples.

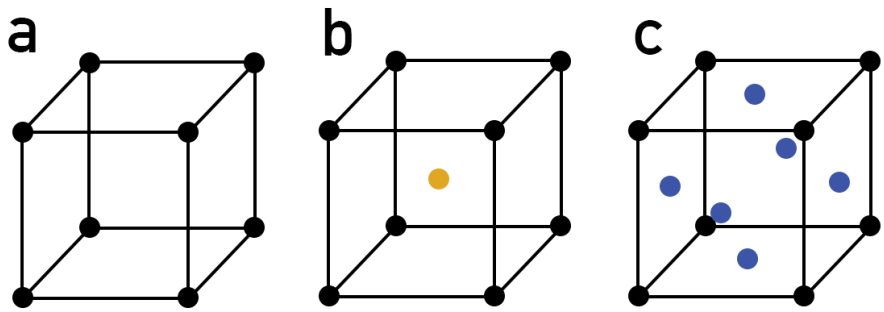

Figure 1: (a)The structure of simple cubic (SC) unit cell. b) Adding one atom in the center of the SC cell gives a body-centered cubic (BCC)) structure. c) Adding an atom to each side of the SC cell gives a face-centered cubic (FCC) structure. The extra atoms compared to the SC structure are colored for clarity, but are still the same type of atom as the SC structure.

Crystalline orientations

The surface structure will depend on the orientation of the lattice relative to the cut of the surface. To study and understand this, there are a few ways to describe crystalline orientations. These can also be used for orientation in the bulk, but this will not be discussed further.

Euler angles

Euler's rotation theorem states that any rotation between unit vectors and a rotated coordinate system in three dimensions can be described using three independent angles. There are multiple ways to define Euler angles depending on rotation sequences and axis conventions, but some are more common than others[2]. One of the most common notations is Bunge's notation, which is what is used in this work. In Bunge's notation, the three Euler angles are φ_1, Φ, and φ_2. Given a system where the coordinate axes are initially defined with $\mathbf{x}$ and $\mathbf{y}$ in the horizontal plane, the φ_1 rotation is a rotation around the initial lab frame z-axis. The Φ rotation is then around the now rotated x-axis. Finally, the φ_2 rotation is around the rotated z-axis. The definition of the coordinate system using Bunge's notation is shown in Figure 2.

Miller indices

Miller indices are a notation of lattice planes, often used to describe the surface plane. The Miller indices (hkl) denote the reciprocals of the fractional intercepts

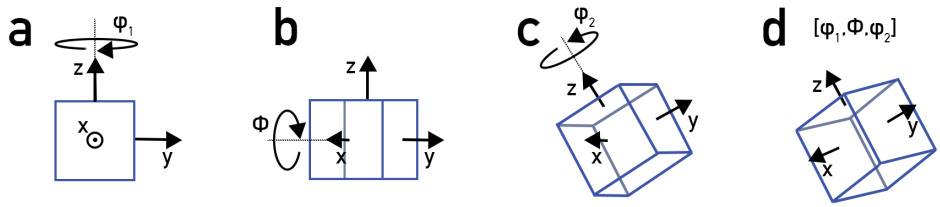

Figure 2: A visualization of Bunge's notation for Euler angles. The coordinate system is rotated with the angle φ_1 around the z-axis (a), then around the x-axis with the angle Φ (b), and finally around the now tilted z-axis with the angle φ_2 (c). d) The final orientation can be described with the vector $[\varphi_1, \Phi, \varphi_2]$.

that a crystal plane makes with the crystallographic axes, expressed in terms of the lattice vectors. A plane parallel to an axis (i.e., no intersection) is assigned an index of 0. In a cubic system, switching the position of two of the indices will result in an equivalent structure since it is only rotated 90° in the unit cell. Thus (100) will give the same surface structure as (010) and (001), and different notations are popular in different fields.

The main low index surfaces or the closely packed surfaces are (100), (110), and (111), all shown for a FCC crystal in Figure 3. These are the only planes in an FCC lattice that are atomically flat without intrinsic steps. The higher index planes can be described as periodic steps with terraces of low index planes. These can be described by their terrace structure, terrace width and step structure. Some high-index surfaces exhibit so-called *kinked* steps which are irregularities along the steps that themselves form miniature facets that can be described by low index facets[3].

For a cubic system, the distance between planes can be calculated as

$$d = \frac{a}{\sqrt{h^2 + k^2 + l^2}}, \tag{2}$$

where a is the lattice constant, i.e., the side of the cube.

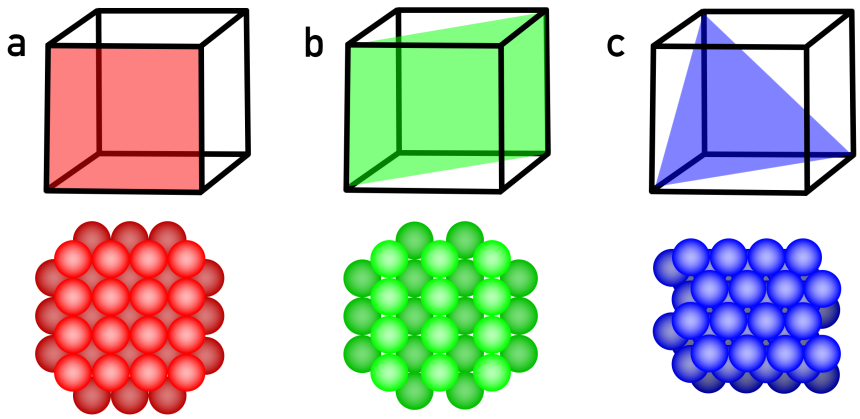

Figure 3: The low index surfaces. The plane drawn for a) (100), b) (110), and c) (111) with the corresponding surface structures for an FCC structure.

Orientation visualization

To visualize surface orientations and to get an understanding of which surface structures are similar, inverse pole figure (IPF) coloring is often used in crystallography. In cubic structures, or more generally those with the $m\bar{3}m$ symmetry group, (100) is colored red, (110) green and (111) is blue. Other orientations can be colored with intermediate hues so that similar orientations are represented by similar colors, allowing for quick visual comparison of grains or surface structures[4]. Figure 4 shows an example created using the Python library Orix[5].

Polycrystalline surfaces and surface dynamics

Polycrystalline surfaces

When discussing polycrystalline surfaces, we refer to samples composed of well-defined domains, or grains, each exhibiting a specific surface orientation. This is illustrated in Figure 4, which shows an IPF map of a polycrystalline surface. While many metals naturally form such grains during solidification, these domains are typically too small (on the order of nanometers to millimeters depending on solidification conditions[6]) to be individually studied with surface-sensitive techniques.

To overcome this limitation, specially prepared model systems are used in which

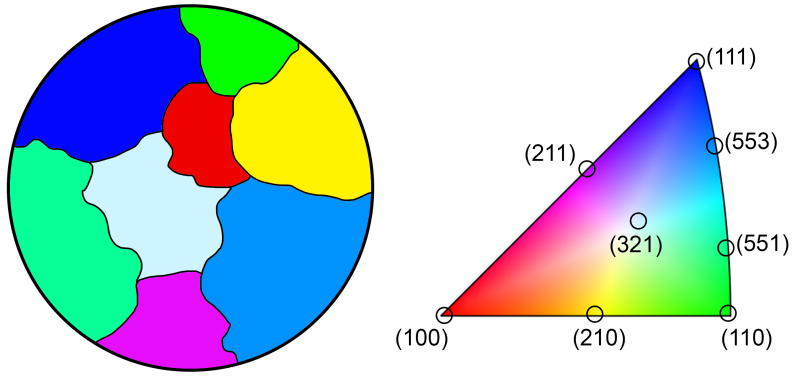

Figure 4: An example of a polycrystalline surface with IPF coloring. The Miller indices corresponding to the grain colors are marked in the IPF triangle. The triangle is created using the Python library Orix[5]

the grain size is increased. These systems enable the study of orientation-dependent surface phenomena under controlled conditions, bridging the gap between ideal single-crystal studies and real-world polycrystalline materials.

Surface changes and palladium

Pd has a high catalytic activity in a wide range of processes. It has, for example, been shown to be one of the most catalytically active materials for CO oxidation and other relevant catalytic reactions[7, 8]. In surface science and catalysis, the following key concepts are often discussed when analyzing such reactions:

Active phase: This refers to the specific state of the catalyst surface under reaction conditions. It may include clean metallic surfaces, surfaces partially covered with adsorbates (e.g. oxygen, hydrogen), or oxidized phases. The active phase can vary significantly with temperature, pressure, and reactant composition. For example, metallic Pd and PdO(101) have been shown to exhibit higher activity than PdO(100) for both CO and CH_4 oxidation[9, 10].

Active sites: These are the specific atomic configurations where reactants adsorb and react[11]. In a catalyst, there will be atoms with varying coordination such as steps, kinks, and flat terraces. This is also true for different surface orientations where for example, Pd(111) has different adsorption properties than Pd(100) or Pd(110).

Surface structures: This includes the long-range order of the surface atoms and any reconstructions or rearrangements that occur under reaction conditions. For instance, Pd surfaces can undergo reconstruction when exposed to oxygen or hydrogen, forming surface oxides or hydride phases that affect catalytic behavior. These changes can also be facet dependent[12].

Understanding these aspects across different crystallographic orientations enables a deeper understanding of structure–reactivity relationships in catalysis. Studies have shown that the reactivity and stability can vary between surfaces like Pd(111), Pd(100), and Pd(110)[13, 14]. SXRD can be useful in studies of surface structures and to some extent active phase, since it can determine long range periodic structures, but not surface adsorbates and adsorption sites.

Related experimental methods

In this chapter, existing methods used in the project are explained. Most importantly, SXRD is the main background method. For the grain mapping, tools from different versions of 3DXRD have also been applied and the basics of these are introduced. At the end there is an introduction to EBSD, which has been used as reference in the development of the grain mapping in Paper **I**.

X-rays and synchrotron radiation

X-rays are electromagnetic radiation with energy between 100 eV and 100 keV (approximately corresponding to wavelengths between 10 nm and 0.1 Å) where the lower end is referred to as soft X-rays and the higher end as hard X-rays. The boundary between soft and hard is not well defined, but usually considered to be around 10 keV. There are many advantages to using X-rays in material and surface science; for instance, large penetration depths (depending on the method) and wavelengths similar to the size object we want to study such as atomic structures.

In a standard lab-based X-ray source, a highly-energetic electron beam hits a metallic target, producing a broad spectrum of bremsstrahlung as well as more intense fluorescence peaks at specific energies. Though limited in, e.g., intensity, resolution, and energy range, these lab sources are very useful for standard studies of bulk structures.

More advanced X-ray sources have, however, enabled more advanced methods. In particular, synchrotron radiation sources have opened up the possibility for a new range of methods and quality of measurements. Synchrotron refers to the type of particle accelerator where particles travels around a closed loop. In the so-called storage ring, different magnets are used to keep the electrons in the correct path. In the first synchrotron X-ray sources, it was the light being

emitted in the bending magnets that was used. When the electrons change direction, X-rays are emitted with a significantly higher intensity than in a lab source. However, more modern sources use insertion devices with a set of magnets that are only used for producing radiation. In an so-called wiggler, a few strong magnets cause a large change of the electron path and hence an intense, broad spectrum. In an so-called undulator, a periodic series of magnets are used, which forces the electron into an oscillating path. The magnetic field is weak, which gives interference between emission from the different bends. As a consequence, the light from an undulator has a very high brilliance for specific wavelengths. At the beamline used for the work included in this thesis, P21.1[15] at PETRA III at DESY in Hamburg, an undulator is used. After the production, a series of monochromator, lenses, slits, etc. are used to define the energy, shape and other properties of the X-ray beam, according to the needs of the method to be used.

Surface X-ray diffraction

Basics of X-ray diffraction

XRD is very useful for studying periodic structures in materials. The oscillating electromagnetic field of the incident beam excites electrons in the material, causing them to oscillate at the same frequency. These oscillations subsequently emit secondary X-rays. When working with XRD, it is assumed that the incoming electromagnetic wave induces a secondary spherical wave at each lattice point in the material. It is also assumed that the scattering is coherent, meaning that there is a fixed phase relationship between the incoming wave and the emitted spherical waves. The interference of the scattered photons results in the diffraction pattern.

Given elastic scattering, the magnitude, k, of the wave vector will be the same before and after scattering, but the direction can be different. This can also be written as $k = |\mathbf{k}| = |\mathbf{k}'| = \frac{2\pi}{\lambda}$, where $\mathbf{k}'$ is the scattered wave vector and λ is the wavelength. XRD can either be described using the Laue condition or Bragg's law, where the latter is a special case of Laue diffraction and provides the scattering angle. The Laue formalism uses the geometry described in Figure 5. The path difference between the X-rays scattered from two atoms separated by a vector $\mathbf{R}$ can be described by

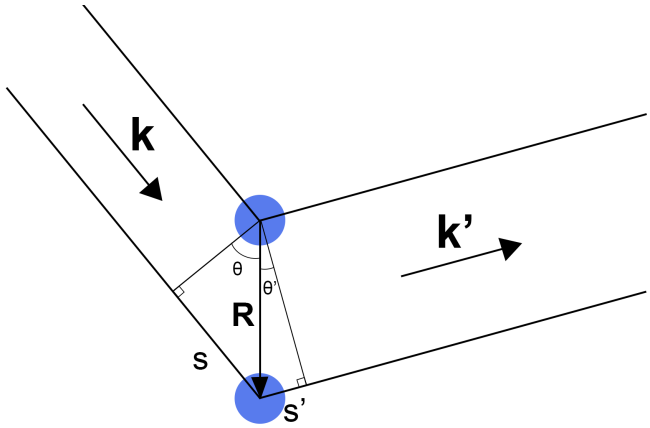

Figure 5: The geometry used to derive the Laue condition. **k** and **k'** are the incoming and outgoing wave vectors, respectively. The vector **R** between lattice points is described by Equation 1.

$$\mathrm{PD} = s' + s = R\cos(\theta') + R\cos(\theta) = \frac{\mathbf{R}\cdot\mathbf{k}'}{k} - \frac{\mathbf{R}\cdot\mathbf{k}}{k} = \frac{\mathbf{R}\cdot\mathbf{Q}}{k}, \tag{3}$$

where $\mathbf{k}' - \mathbf{k} = \mathbf{Q}$, also known as the scattering vector. To have constructive interference the path difference should be an integer multiple of the wavelength, that is,

$$PD = n\lambda = n\frac{2\pi}{k}. \tag{4}$$

Combining Equation 3 and 4 gives that

$$\mathbf{Q}\cdot\mathbf{R} = 2\pi n. \tag{5}$$

In order to have full constructive interference in the whole lattice, Equation 5 must be fulfilled for any lattice vector $\mathbf{R}$ defined in Equation 1 (i.e., for any integers m_1, m_2, and m_3).

We now define the reciprocal lattice corresponding to the real lattice defined in Equation 1 as

$$\mathbf{G} = n_1\mathbf{b}_1 + n_2\mathbf{b}_2 + n_3\mathbf{b}_3, \tag{6}$$

where $\mathbf{b}_i$ are the reciprocal lattice basis vectors and n_i are integers. The reciprocal lattice is related to the real lattice by $\mathbf{a}_i\cdot\mathbf{b}_j = 2\pi\delta_{ij}$. Both $\mathbf{k}$, $\mathbf{k}'$ and $\mathbf{Q}$ can be described using these reciprocal basis vectors. With $\mathbf{Q} = h\mathbf{b}_1 + k\mathbf{b}_2 + l\mathbf{b}_3$, Equation 5 gives

$$2\pi n = \mathbf{Q}\cdot\mathbf{R} = (h\mathbf{b}_1 + k\mathbf{b}_2 + l\mathbf{b}_3)\cdot(m_1\mathbf{a}_1 + m_2\mathbf{a}_2 + m_3\mathbf{a}_3) = 2\pi(m_1h + m_2k + m_3l). \tag{7}$$

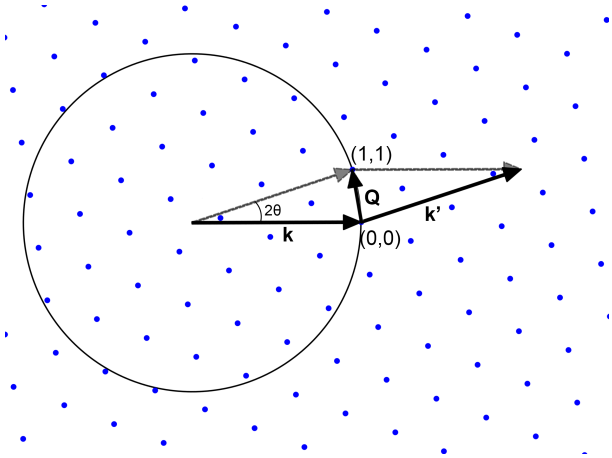

Figure 6: Example of an Ewald circle (Ewald sphere in two dimensions). In this example, the conditions for diffraction from the (h,k)=(1,1) point in a hexagonal reciprocal lattice is shown.

This entails that, in order to get full constructive interference, h, k[1], and l must be integers. Thus, to get positive interference, the change in the wave vector $\mathbf{Q}$ must be a reciprocal lattice vector $\mathbf{G}$.

In Laue diffraction, it is common to use the Ewald sphere, which describes which points in reciprocal space can be reach by $\mathbf{Q}$, with a specific length and direction of $\mathbf{k}$ and any possible direction of $\mathbf{k}'$. In order to probe a certain point in the reciprocal lattice, the lattice is rotated such that this point intersects the sphere. When this happens, diffraction will occur. An example is shown in Figure 6 in two dimensions, where the Laue condition can be found to be fulfilled for a certain angle for $\mathbf{k}'$ when the lattice is rotated such that a reciprocal lattice point intersects the circle. This angle dependence of fulfilling the Laue condition is important if you do any type of diffraction, with the exception of powder diffraction. In a powder sample, all crystalline orientations will be present, and a single shot at a single angle is typically enough. For a single crystal, some rotation of the sample/detector is needed to measure the whole structure.

A more realistic description of materials than point scatterers are spatially extended electron density distributions. This is accounted for using the atomic form factor, $f^0(Q)$, which essentially results in a gradual drop in scattered intensity as Q (or the scattering angle) increases. For a crystal with more than

[1]Note here that k in Equation 7 is not the length of wave vector but an integer describing a point in the reciprocal lattice. This notation might be confusing but it is standard.

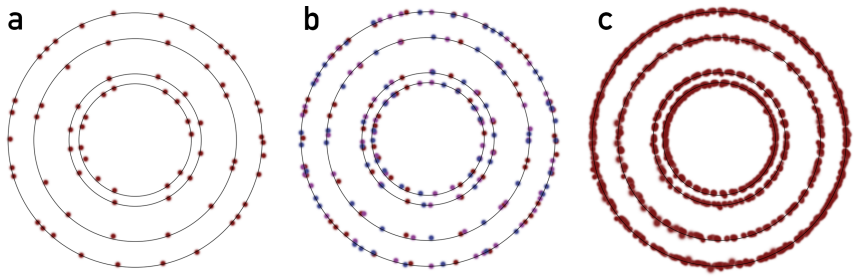

Figure 7: Example of diffraction patterns. a) Diffraction from a single crystal with discrete Bragg spots. The rings mark the Debye-Scherrer rings. b) Diffraction from a polycrystalline sample where the colors mark diffraction spots from different grains. c) Powder diffraction where full rings are formed.

one atom in the unit cell, the form factor can be described as

$$F(\mathbf{Q}) = \sum_j f_j(\mathbf{Q}) e^{i\mathbf{Q}\cdot\mathbf{r}_j} \sum_n e^{i\mathbf{Q}\cdot\mathbf{R}_n}, \tag{8}$$

where the first sum, or structure factor, describes how the intensity of different diffraction spots varies due to the position of the atoms inside the unit cell, while the second sum, or lattice sum, specifies that h, k and l need to be integers, as described above.

For powder diffraction, where the sample is a powder with all possible crystalline orientations, the diffraction will result in hollow cones that, if measured with a two dimensional detector, will be seen as rings known as Debye-Scherrer rings. The scattering angle, 2θ, is the angle between $\mathbf{k}$ and $\mathbf{k}'$, that describes the ring spacing. θ can be calculated using Bragg's law

$$n\lambda = 2d\sin(\theta), \tag{9}$$

where n is the diffraction order, λ is the wavelength, and d is the lattice spacing of some plane in the crystal (see Equation 2). Also polycrystalline samples and single crystals will show the same rings but more sparse. Since the orientation of these samples are fixed, the Bragg spots will appear at specific azimuthal angles, η, that depend on surface orientation. The difference between diffraction from a single crystal, polycrystal, and a powder sample is shown in Figure 7, where the former two are assumed to have been rotated around the vertical axis.

Surface X-ray diffraction

So far, this has been a general description of diffraction. In this section, we focus on SXRD, a technique for studying the atomic structure of surfaces and interfaces. Two relevant cases can be considered: diffraction from a truly two-dimensional (2D) system and diffraction from the surface of a bulk crystal.

In the first case, the crystal structure lacks periodicity along the surface normal, i.e., there is no basis vector $\mathbf{a}_3$. For this structure, Equation 7 will instead be

$$2\pi n = \mathbf{Q} \cdot \mathbf{R} = (h\mathbf{b}_1 + k\mathbf{b}_2 + l\mathbf{b}_3) \cdot (m_1\mathbf{a}_1 + m_2\mathbf{a}_2) = 2\pi(m_1 h + m_2 k), \quad (10)$$

and the diffraction becomes independent of the index l. The resulting diffraction pattern consists of rods in reciprocal space perpendicular to the surface plane, described as

$$\mathbf{Q}_{||} = \mathbf{G}_{hk} = h\mathbf{b}_1 + k\mathbf{b}_2, \quad (11)$$

where (h, k) are the in-plane indices and $\mathbf{b}_i$ are the reciprocal lattice vectors.

In the second case, where a 2D surface is the termination of a three-dimensional (3D) crystal, these rods extend continuously through reciprocal space and intersect the positions of bulk Bragg peaks. This extended feature is known as crystal truncation rod (CTR). They arise due to the termination of the otherwise periodic crystal lattice at the surface, which can be described as the multiplication of a perfect bulk crystal by a step function in real space. In reciprocal space, this convolution broadens the sharp Bragg points into rods. The intensity distribution along the rods provides direct information about the atomic structure near the surface, including relaxations and reconstructions[16, 17].

For surfaces that are not atomically flat, but composed of tilted facets, the resulting truncation rods are likewise tilted. The angular deviation of these rods reflects the average orientation of the facets. This effect allows SXRD to probe facet distributions. If the surface exhibits a reconstruction or there is an additional thin layer (such as an oxide), the periodicity may differ from that of the bulk. In such cases, additional rods appear at fractional in-plane positions, known as superstructure rods (SSRs). These do not necessarily intersect any bulk Bragg positions and contain information about the reconstructed or adsorbed layer. If a surface oxide grows into a bulk oxide, new Bragg spots will appear. Surface roughness and finite domain sizes also influence the diffraction pattern. Roughness leads to a decay in CTR intensity due to destructive interference between terraces with different heights.

The surface sensitivity of SXRD stems from the separation of the bulk information (Bragg spots) and surface information (CTRs and SSRs). Sufficient surface

structure intensity is achieved by limiting the penetration depth of the X-ray beam. The incidence angle α is kept below or close to the critical angle α_c for total external reflection, typically less than 1° for hard X-rays. The refractive index n in the X-ray regime is expressed as

$$n = 1 - \delta + i\beta, \tag{12}$$

where δ is related to the dispersion and β the absorption, which will be neglected now when looking at the critical angle. δ is described

$$\delta = \frac{n_a r_e \lambda^2}{2\pi} f_1, \tag{13}$$

where n_a is the number density, r_e the electron radius and f_1 is one of the components of the atomic scattering factor, $f = f_1 + f_2$. There is a dependence of f_1 on X-ray energy, but the main factor determining how δ varies is λ, which results in a decrease at higher energies. The critical angle can be approximated by

$$\alpha_c \approx \sqrt{2\delta}, \tag{14}$$

and will thus be almost inversely proportional to the photon energy. Below this angle, the X-ray field decays exponentially into the material as

$$I = I_0 e^{-x/\Lambda}, \tag{15}$$

where Λ is the elastic mean free path (EMFP). The effective probing depth typically ranges from a few nanometers up to several tens of nanometers.

A key consequence of grazing incidence is the elongation of the beam footprint:

$$F = \frac{D}{\sin(\alpha)}, \tag{16}$$

where D is the incident beam height, as shown in Figure 8c. At shallow angles, the footprint may extend several centimeters in length, even for a narrow beam. This limits spatial resolution and typically restricts the use of SXRD to single crystals or large, uniform domains.

In this work, we use high energy surface X-ray diffraction (HESXRD) in combination with a flat 2D detector while rotating the sample to fulfill the Laue condition at different angles. The HESXRD setup allows for fast data acquisition of full diffraction patterns. The higher energy of the synchrotron beam gives a flatter Ewald sphere. A CTR will fully intersect the sphere in just a few degrees[18]. The high brilliance allows for measurements of surface structures with good signal-to-noise, but also brings the risk of detector damage from

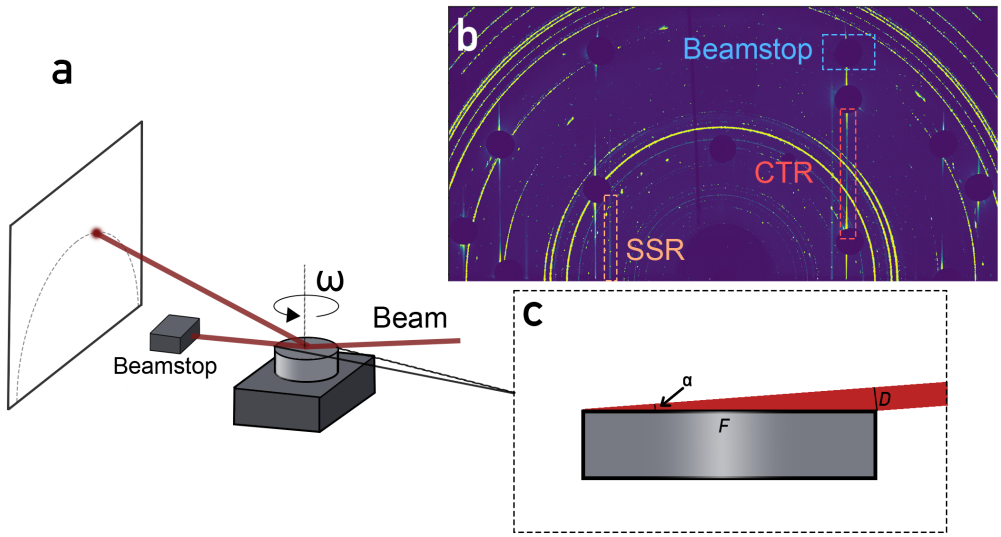

Figure 8: Sketch of SXRD setup. a) An example of a SXRD setup with a large 2D detector. ω is the rotation angle. b) An example of a SXRD measurement of a single crystal where beamstops mask the Bragg spots. Both CTRs and SSRs are visible. The rings intersecting the Bragg spots are powder diffraction from the sample indicating an imperfect single crystal and the rings not intersecting the Bragg spots are powder diffraction from other parts of the setup. c) A sketch showing why an angle of grazing incidence will give a footprint, F, covering a large part of the sample length even if the beam height, D, is smaller than the sample.

intense bulk Bragg reflections. These strong peaks are often masked or attenuated in surface-sensitive measurements to protect the detector and focus on the weaker surface signal. Figure 8 shows a typical HESXRD setup and an example result, illustrating the appearance of CTRs and SSRs.

Three-dimensional X-ray diffraction

3DXRD refers to a class of non-destructive techniques used to study the internal grain structure and orientations of polycrystalline materials in three dimensions. While 3DXRD often refers to 3DXRD microscopy, several related techniques exist, including diffraction contrast tomography (DCT) and scanning 3DXRD. This section introduces the principles of 3DXRD microscopy, with a particular focus on the indexing tool GrainSpotter, and provides an overview of scanning 3DXRD and DCT as complementary methods.

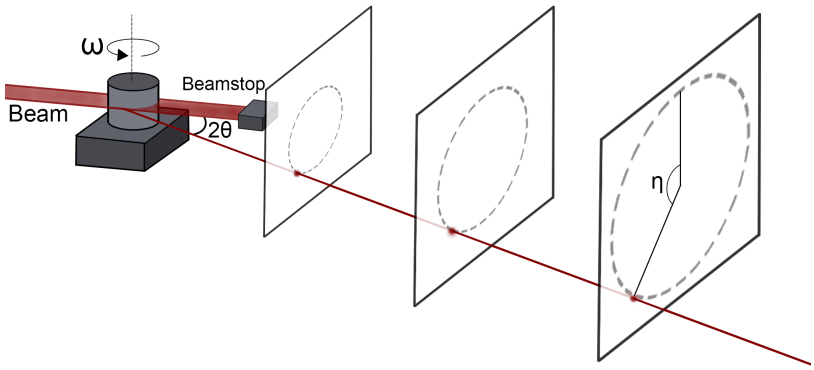

Figure 9: A typical 3DXRD microscopy setup, here using an X-ray sheet. The detector is shown at three different SDDs, to show the principle of ray tracing.

3DXRD microscopy

In most 3DXRD approaches, a setup as shown in Figure 9 is used. The X-ray beam can either be focused to a sub-volume, shaped as a plane, or used to illuminate the entire sample. The sample is mounted on a rotation stage, and diffraction patterns are collected as the sample rotates.

Many 3DXRD approaches use either several 2D detectors at different sample detector distances (SDDs)[2] or one 2D detector that is moved to different SDDs. Looking at the methodology used in GRAINDEX [19, 20, 21], the original program for this purpose, the rotations of the sample are combined with measurements at different SDD. This allows for ray tracing by fitting a straight line through the center of mass (COM) of equivalent Bragg spots which can be extrapolated to the point where the line intersects with the measured plane. These lines can then provide the COM of the corresponding grain. Each detected Bragg spot can be described by its scattering angle 2θ and an azimuthal angle η, which are used to determine the corresponding reciprocal lattice vector $\mathbf{G}$, through

$$\mathbf{G} = \frac{2\pi}{\lambda} \begin{pmatrix} \cos(2\theta) - 1 \\ -\sin(2\theta)\sin(\eta) \\ \sin(2\theta)\cos(\eta) \end{pmatrix}. \tag{17}$$

The orientation of the grain can then be found. This 3DXRD approach can also provide information such as strain. Using a focused beam allows for grain

[2]The distance can be referred to as *rotation axis to detector distance* since the sample has a thickness.

shape determination using back-projection. Since 3DXRD requires transmission of X-rays through the sample, there is a limit on sample size.

The advantage of 3DXRD is the ability to study grains of materials in three dimensions in a non-destructive manner. As for the grain mapping in Paper **I**, the 3DXRD methods are often compared with EBSD measurements during the development. Since 3DXRD measures 3D crystals, they use focused ion beam (FIB) milling to be able to grain map each layer of the crystal with EBSD scans.

GrainSpotter

For the grain mapping in Paper **I**, we have adapted parts of GrainSpotter [22], a fairly modern algorithm for finding grains, to a surface system. In GrainSpotter, the whole sample should be within the beam throughout the rotation. The algorithm identifies grains by searching for overlaps in orientation space using Rodrigues vectors, an alternative to Euler angles. While the Euler angles describe three rotations around basis vectors, Rodrigues notation combines these rotations into one, around a single unit vector $\mathbf{k}$. The angle of rotation, ϕ, is included as the length of the Rodrigues vector such that the change in orientation can be represented by a single 3D vector, the Rodrigues vector:

$$\mathbf{r} = \tan(\phi/2)\mathbf{k}. \tag{18}$$

This representation allows each grain to be described as a point in Rodrigues space.

To locate grains in real space, the diffraction spots are first converted into reciprocal scattering vectors (**G**-vectors) under the assumption that all grains are at the COM of the sample. Each diffraction spot generates a geodesic (a line in Rodrigues space) representing the set of orientations for which that diffraction condition is satisfied. GrainSpotter finds common intersections of multiple geodesics, which correspond to possible grain orientations. The grain orientations are determined as the points where multiple geodesics intersect, since only a correct orientation will satisfy multiple diffraction conditions. However, noise and intensity variations can lead to missing **G**-vectors for a grain. A completeness threshold can therefore be used to set a reasonable limit on the allowed missing diffraction spots.

Once an orientation is found, the algorithm predicts where the diffraction spots should appear if the grain were at the sample's center. If the actual diffraction spots do not perfectly match the expected positions, the grain is not at the assumed center. The algorithm then adjusts the grain's position iteratively

to minimize the difference between observed and predicted diffraction spots. Mathematically, this is done by minimizing the perpendicular distance between the detected diffraction rays and the grain's assumed position. The least-squares fitting method is used to find the best position for each grain.

Additionally, GrainSpotter applies pseudo-twin analysis to eliminate erroneous grains. Pseudo-twins are orientations with partial overlap of diffraction spots. Even though there should be a overlap of <30% of the **G**-vectors, lower completeness of grains or wrongly assigned **G**-vectors can result in a higher pseudo-twin completeness. The final output includes a list of grains with their orientations and COM positions.

Scanning 3DXRD microscopy

Another approach for 3D-mapping of samples, developed by Hayashi et al., is scanning 3DXRD microscopy[23]. In their approach, a focused X-ray beam is used with a size smaller than the grains. The sample is measured in horizontal layers with a measurement procedure similar to what is used in Paper **I**. The sample is moved perpendicular to the beam, such that the beam moves from edge to edge of the sample, with a rotation at each translation step. After a scan from edge to edge the sample is moved vertically such that a new slice can be measured. The horizontal step size is the same as the beam width and the vertical size the beam height.

For a point $Q(x, y, z)$ in the sample, the subset of **G**-vectors can be extracted where this point has been measured. An indexing can be performed for this point giving a small selection of grains. The grain that shows the highest completeness, defined as $N_{\text{measured}}/N_{\text{theoretical}}$, is assigned to the point. Here, N is the number of **G**-vectors for one grain. This can be repeated for the whole sample in a pixel-by-pixel approach. Scanning 3DXRD microscopy has some advantages, such as less issues with overlapping Bragg spots than with wide beam approaches, and it can measure thicker specimens than other 3DXRD methodologies.

Diffraction contrast tomography

DCT is a synchrotron-based technique related to 3DXRD microscopy. It detects grains by measuring extinction contrast in the transmitted X-ray beam when a grain satisfies the Laue diffraction condition. By acquiring images over a rotation range, the grain shapes are reconstructed via tomographic back-projection. Grain orientations are determined by associating diffraction spots

across multiple projections during a mapping stage. DCT is particularly suited for low-strain, near-pure materials with well-separated grains, and complements 3DXRD microscopy by providing full grain shape reconstructions with high spatial resolution[24].

Electron Backscatter Diffraction

EBSD is an additional technique that can be integrated into a scanning electron microscope (SEM)[25, 26]. It is primarily used for polycrystalline samples to determine grain orientations, textures, and other crystallographic information. Since SEMs are widely available and EBSD analysis is largely automated, EBSD is a highly accessible method. In this section, EBSD is mainly described as a grain mapping tool.

EBSD analysis is based on the detection of Kikuchi patterns, which enable the determination of crystal orientation from a single measurement. For this reason, EBSD is sometimes also referred to as backscatter Kikuchi diffraction. During EBSD acquisition, the sample is tilted to approximately 70° (placing the surface at a 20° angle relative to the electron beam), as shown in Figure 10a. The incident electrons undergo primarily incoherent scattering with minimal energy loss, also known as quasi-elastic scattering. This interaction can be viewed as generating an effective electron source within the near-surface scattering volume.

The electrons are scattered in all directions and will thus also interact with planes in all directions. Electrons satisfying Bragg's law for a given plane will form two large-angle diffraction cones, as shown in Figure 10b. When these cones intersect the 2D detector, they appear as thin lines called Kikuchi lines. Kikuchi patterns consist of pairs of Kikuchi lines that form bands. The width of each band is related to the inter-planar spacing, d_{hkl}. These bands will be formed for all families of crystallographic planes. Where multiple bands intersect, they define a zone axis, since the corresponding planes share a common crystallographic direction. By identifying the zone axis and the orientation of the bands relative to the detector, the crystal orientation can be determined. For a given crystal structure (e.g., FCC), the angles between bands are fixed and independent of the sample's surface orientation[25, 27].

EBSD requires samples to meet specific surface and environmental conditions. The surface must be relatively flat, and there are limitations on the amount of residual stress the sample can tolerate. The sample must also meet the general requirements for SEM imaging; most notably, it must be electrically conductive.

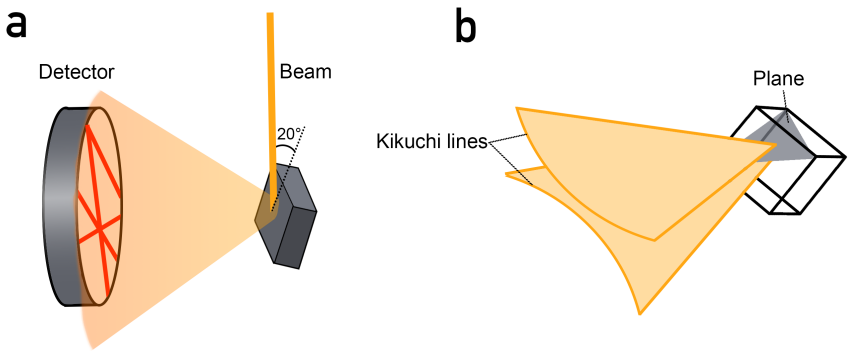

Figure 10: EBSD setup. a) General EBSD setup with the sample tilted with an approximate angle of 20° relative to the electron beam. b) Sketch of Kikuchi lines from one plane.

Although SEM beams can be focused down to tens of nanometers, the spatial resolution of EBSD is not determined solely by the beam size. Instead, it is governed by the size of the excitation volume, which is the region where diffraction occurs and electrons exit the sample without further interactions. The penetration depth depends on the mean free path, which in turn is influenced by the beam energy. While reducing the accelerating voltage can decrease the excitation volume, it may also reduce pattern quality. At typical accelerating voltages (around 20 kV), the excitation depth is on the order of tens of nanometers[26].

Tomography

The word tomography has its origin in Greek from *tomos* meaning "slice" or "section" and *graphia* meaning "description of", but can also be said to stem from a more modern version meaning "to record" or "to write". In modern usage, it generally refers to the process of imaging by sections or slices through an object, typically to reconstruct a 3D representation.

Tomography has a wide range of applications, from medical imaging techniques such as computed tomography (CT) to materials science, geophysics, and archaeology. While many tomographic methods rely on absorption contrast using penetrating radiation such as X-rays, this is not universally true. What all tomography techniques have in common is the reconstruction of a 3D volume from a set of 2D measurements or "slices"[28].

Some reconstruction methods use direct Fourier-based approaches to retrieve the

real-space object. However, it is common to instead use some form of projection approach. In these methods, the measurements are treated as line integrals, which are values representing a physical property (like attenuation or density) integrated along a line through the object at a given angle. By collecting these line integrals from many angles, it becomes possible to reconstruct the internal structure of the object using techniques such as filtered back-projection or iterative reconstruction algorithms[28]. Simple back-projection is simply to assign the 2D projection to all voxels along the line path.

Tomographic Surface X-ray Diffraction

The aim of the work reported in this thesis is to develop TSXRD in order to allow SXRD to be applied to polycrystalline surfaces. The approach of TSXRD can be divided into two steps:

1. Mapping the surface of the polycrystalline sample using Bragg reflections
2. Sorting SXRD signals by assigning them to the grains of the sample

These are presented in Paper **I** and Paper **II**, respectively. Here, a summary of the whole approach will be given.

As described above, the angle of grazing incidence of a SXRD setup will result in a long beam footprint. Even when a small beam is used, we will measure several grains in the beam direction. To get full diffraction measurements of the polycrystalline sample, each part of the surface needs to be measured at an angular range large enough to measure the full crystalline structure. A single sample rotation, which is what is typically used for single crystal SXRD with a large 2D detector, only the small area around the rotational axis will be fully measured, given that the beam is aligned with the rotational axis. Note that while this area will be fully measured, there will be additional diffraction from a slice along the sample at each angle. To fully measure the sample, it is moved stepwise from edge to edge in the y-direction perpendicular to the beam. The movement in y is performed using a motor below the rotation stage. The sample will therefore always rotate around the same rotational axis, aligned to the sample center, but the beam position will be moved with each y-step. A rotation scan — a continuous rotation at a range $-\omega$ to ω with measurements every $\Delta\omega$— is performed after each y-step, resulting in a scanning pattern that,

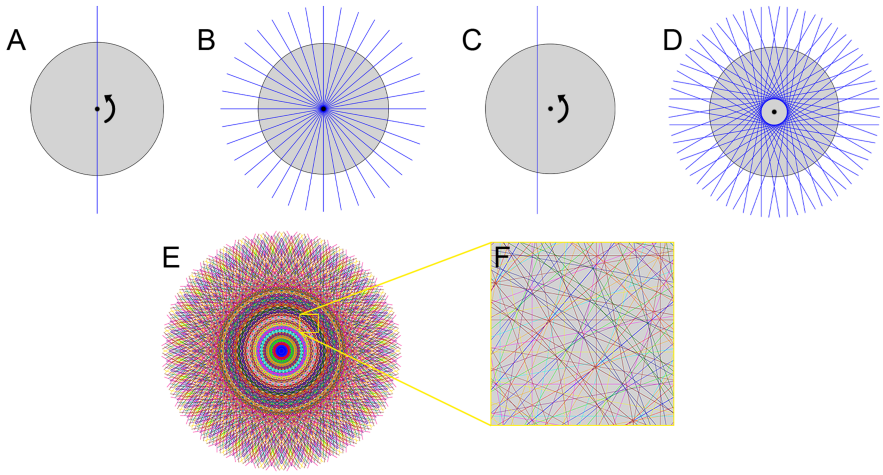

Figure 11: The measurement procedure for TSXRD. A-B) Rotation with the beam at the rotational axis will result in a full measurement of the center of the sample. C-D) Moving the sample perpendicular to the beam below the rotational stage will result in a rotation with the beam off the rotational axis. E-F) Combining a large range of y-steps and angular steps will give a full measurement of the sample.

with small enough $\Delta\omega$ and Δy steps, will give a full measurement of the sample as shown in Figure 11.

The analysis procedure for creating grain maps is explained in detail in Paper **I**. The full selection of **G**-vectors from all measurements of the samples are analyzed using GrainSpotter[22] to find all grain orientations. In this analysis, multiples of the same **G**-vector are combined since most Bragg spots will appear in consecutive y-steps if the grain of origin is wider than the beam. To determine the grain map for a grain, the expected **G**-vectors for the grain are compared to the **G**-vectors from all measurements. Each **G**-vector will give both a range of y-positions and the rotational angle, ω, where the grain was measured. This together with the known beam width will give a line in the sample coordinate space for each **G**-vector, which when combined with all **G**-vectors for the grains gives a map where the intensity in each voxel of the surface is the completeness of the given grain in that point, if normalized with the expected number of **G**-vectors for the grain. Placing a completeness threshold on the map will then give a grain contour.

After the completeness threshold, there will still often be an overlap of neighboring grains. This is both due to a general uncertainty in the grain boundary region due to a higher presence of imperfections, and a smudging of the completeness map due to the long beam footprint. To determine the most likely grain in each point of the surface, the completeness is used as a selection cri-

teria. If the completeness map is used directly, larger grains have a tendency to have an exaggerated size at the expense of smaller grains. This is an effect that is also discussed in relation to scanning 3DXRD microscopy, that has a very similar measurement and analysis approach[23]. Our solution is to, before comparing the completeness maps of the grains, multiply them with a correction term

$$C_{corr} = \frac{1}{\sqrt{C_{max}\sqrt{r}}} \tag{19}$$

where C_{max} is the maximum completeness of the grain and r is the approximate grain radius. After correction, the grains can be combined into a grain map with both known grain shapes and grain orientation.

As described for HESXRD, the Bragg reflections are often too intense to be measured simultaneously with the surface signals. The grain mapping is thus either done with attenuators in the beam or with a deliberately detuned undulator gap. To measure the surface signals, the Bragg spots are covered as shown in Figure 8, but since the sample is now polycrystalline, it is inefficient to cover each Bragg spot individually. Instead, circular masks along the Debye-Scherrer ring are used, which cover all spots from a given material.

The surface signals are measured with the same measurement procedure as for the Bragg reflections described in Figure 11. The surface signals can be sorted using the angle dependence of the diffraction signal. At a given angle, the same part of a surface signal should be present at all translations where the beam is measuring the same grain, so at each angle, a projection of all grains is extracted from the grain map. The occurrence of a group of pixels in consecutive y-steps is compared with the grain projections. An example of a projection comparison is shown in Figure 12. If there is a tie between two grains in this comparison, the signal is assigned to both. A complete overlap should only occur at a very small angular range and only a small part of, for example, a CTR should therefore be wrongly assigned. After the assignment has been performed at all angles, such issues can be managed by discarding signals that are too small when combining it with the rotation.

Outlook

As discussed in the introduction, the goal with TSXRD is polycrystalline SXRD *operando* measurements. Here, the basics of the approach have been presented with *ex situ* examples. The next steps are to apply the method in interesting *operando* studies. The measurement procedure presented here, where the whole

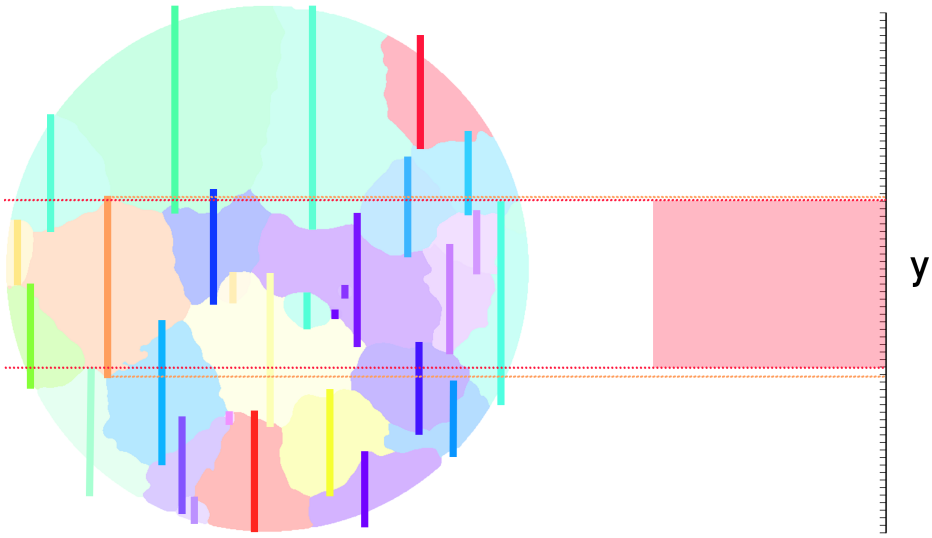

Figure 12: An example of the projection approach in TSXRD. The 2D projection of each grain at a given angle is shown as lines over the grain map. A signal present in images marked with the red square are compared with the grain projections. In this example, the signal is most likely to belong to the orange grain.

sample is measured at all angles, is quite time-consuming (45 minutes to 2 hours for the 7 mm Pd sample, depending on angular range and exposure time). Therefore, this full scan process is only useful for stable structures, which is not always the case for intermediate states such as thin surface oxides. We suggest a few different solutions depending on time resolution needs.

An initial sorting of signals can be used as a mask for faster measurements. Instead of fully measuring the surface at different conditions, the grains can be measured with just one rotation each, and the signal can be sorted based on the results of the clean surface. This reduces the time to approximately 1 minute/grain. One challenge is then the sorting of new signals appearing during the reaction, and the approach might have to be supported with more full measurements at different conditions. To save more time, the angular range can be reduced to follow the changes in a few selected signals. A single CTR can be measured with just a few degrees rotation, which brings the time resolution down to seconds/grain.

An important motivation for a method like this is that it will take advantage of fourth generation synchrotron light sources. The increased brightness will allow for much shorter exposure times, and the maps that now take hours could possibly be achieved in minutes. This, of course, requires that the rest of the setup can handle the faster measurements. For example, the rotation stage will

have to rotate very fast without compromising on the stability, which is very important when working with SXRD. This can also be combined with other time-saving measures, such as the ones listed in the previous paragraph, to get more surface information in a shorter time.

With this, systems such as the one measured with surface optical reflectance in reference 12 can be studied. This is a proof of concept for surface optical reflectance as a method for simultaneously studying many surface orientation under realistic conditions[12]. The method uses the change in reflectivity to follow changes in all grains, and they can connect the result to the grain orientations by comparing it to an EBSD map. In the example they study a polycrystalline Pd surface during CO oxidation, which is a good model reaction.

Summary of Papers

Paper I

Surface grain orientation mapping using grazing incidence X-ray diffraction
This paper presents the first step in the development of TSXRD. To give a base for the SXRD measurements, grain maps are here created using Bragg reflections from measurements with a SXRD setup. The paper introduces both a measurement procedure and an analysis approach. The result is grain shapes and orientations on a polycrystalline surface. The grain maps are compared to maps of the same sample obtained with EBSD.

Paper II

Tomographic surface X-ray diffraction - A method for studying polycrystalline surfaces
The focus in this paper is the approach for sorting CTRs and other surface signals to assign them to the grains mapped in Paper **I**. This is initially done with the same clean Pd sample as in Paper **I** in order to be able to compare assigned surface structures to the Bragg spots of the bulk. This allows for determination of both the completeness of the assigned diffraction pattern and the accuracy of the sorting. The method was also applied to the surface after three different O_2 exposures, to show the possiblity of following changes at the surface.

References

[1] J. K. Nørskov, A. Latimer, and C. F. e. Dickens, "Research Needs Towards Sustainable Production of Fuels and Chemicals," tech. rep., 2019.

[2] R. L. Pi0, "Euler Angle Transformations," Tech. Rep. 4, 1966.

[3] M. A. Van Hove and G. A. Somorjai, "A new microfacet notation for high-Miller-index surfaces of cubic materials with terrace, step and kink structures," *Surface Science*, vol. 92, pp. 489–518, 2 1980.

[4] G. Nolze and R. Hielscher, "Orientations - Perfectly colored," *Journal of Applied Crystallography*, vol. 49, pp. 1786–1802, 10 2016.

[5] D. N. Johnstone, B. H. Martineau, P. Crout, P. A. Midgley, and A. S. Eggeman, "Density-based clustering of crystal (mis)orientations and the orix Python library," *urn:issn:1600-5767*, vol. 53, pp. 1293–1298, 9 2020.

[6] M. Wang and B. Duan, "Materials and Their Biomedical Applications," *Encyclopedia of Biomedical Engineering*, vol. 1-3, pp. 135–152, 1 2019.

[7] L. C. Grabow, B. Hvolbæk, and J. K. Nørskov, "Understanding trends in catalytic activity: The effect of adsorbate-adsorbate interactions for Co oxidation over transition metals," *Topics in Catalysis*, vol. 53, pp. 298–310, 5 2010.

[8] M. Hartings, "Reactions coupled to palladium," *Nature Chemistry 2012 4:9*, vol. 4, pp. 764–764, 8 2012.

[9] J. Gustafson, O. Balmes, C. Zhang, M. Shipilin, A. Schaefer, B. Hagman, L. R. Merte, N. M. Martin, P. A. Carlsson, M. Jankowski, E. J. Crumlin, and E. Lundgren, "The Role of Oxides in Catalytic CO Oxidation over Rhodium and Palladium," *ACS Catalysis*, vol. 8, pp. 4438–4445, 5 2018.

[10] S. Yang, A. Maroto-Valiente, M. Benito-Gonzalez, I. Rodriguez-Ramos, and A. Guerrero-Ruiz, "Methane combustion over supported palladium catalysts: I. Reactivity and active phase," *Applied Catalysis B: Environmental*, vol. 28, pp. 223–233, 12 2000.

[11] C. Vogt and B. M. Weckhuysen, "The concept of active site in heterogeneous catalysis," *Nature Reviews Chemistry 2022 6:2*, vol. 6, pp. 89–111, 1 2022.

[12] S. Pfaff, A. Larsson, D. Orlov, L. Rämisch, S. M. Gericke, E. Lundgren, and J. Zetterberg, "A Polycrystalline Pd Surface Studied by Two-Dimensional Surface Optical Reflectance during CO Oxidation: Bridging the Materials Gap," *ACS Applied Materials and Interfaces*, vol. 16, pp. 444–453, 1 2024.

[13] W. Dong, V. Ledentu, P. Sautet, A. Eichler, and J. Hafner, "Hydrogen adsorption on palladium: a comparative theoretical study of different surfaces," *Surface Science*, vol. 411, pp. 123–136, 8 1998.

[14] X. Xu, J. Szanyi, Q. Xu, and D. W. Goodman, "Structural and catalytic properties of model silica- supported palladium catalysts: a comparison to single crystal surfaces," *Catalysis Today*, vol. 21, pp. 57–69, 8 1994.

[15] Z. Hegedüs, T. Müller, J. Hektor, E. Larsson, T. Bäcker, S. Haas, A. L. Conceiçao, S. Gutschmidt, and U. Lienert, "Imaging modalities at the Swedish Materials Science beamline at PETRA III," *IOP Conference Series: Materials Science and Engineering*, vol. 580, p. 012032, 8 2019.

[16] I. K Robinson and D. J. J. Tweet, "Surface X-ray diffraction," tech. rep., 1992.

[17] E. Conrad, "Diffraction Methods," *Handbook of Surface Science*, vol. 1, pp. 271–360, 1 1996.

[18] J. Gustafson, M. Shipilin, C. Zhang, A. Stierle, U. Hejral, U. Ruett, O. Gutowski, P. A. Carlsson, M. Skoglundh, and E. Lundgren, "High-energy surface x-ray diffraction for fast surface structure determination," *Science*, vol. 343, pp. 758–761, 2 2014.

[19] E. M. Lauridsen, S. Schmidt, R. M. Suter, and H. F. Poulsen, "Tracking: a method for structural characterization of grains in powders or polycrystals," *Journal of Applied Crystallography*, vol. 34, pp. 744–750, 12 2001.

[20] H. F. Poulsen, "3DXRD: Grain maps, grain dynamics and grain refinements," *Crystallography Reviews*, vol. 10, pp. 29–43, 1 2004.

[21] H. F. Poulsen, S. F. Nielsen, E. M. Lauridsen, S. Schmidt, R. M. Suter, U. Lienert, L. Margulies, T. Lorentzen, and D. Juul Jensen, "Three-dimensional maps of grain boundaries and the stress state of individual grains in polycrystals and powders," *Journal of Applied Crystallography*, vol. 34, pp. 751–756, 12 2001.

[22] Schmidt, "GrainSpotter: a fast and robust polycrystalline indexing algorithm," *Journal of Applied Crystallography*, vol. 47, pp. 276–284, 2014.

[23] Y. Hayashi, Y. Hirose, and Y. Seno, "Polycrystal orientation mapping using scanning three-dimensional X-ray diffraction microscopy," *Journal of Applied Crystallography*, vol. 48, pp. 1094–1101, 8 2015.

[24] W. Ludwig, S. Schmidt, E. M. Lauridsen, and H. F. Poulsen, "X-ray diffraction contrast tomography: a novel technique for three-dimensional grain mapping of polycrystals. I. Direct beam case," *Journal of Applied Crystallography*, vol. 41, pp. 302–309, 4 2008.

[25] G. Nolze, T. Tokarski, and Rychłowski, "Use of electron backscatter diffraction patterns to determine the crystal lattice. Part 1. Where is the Bragg angle?," *Journal of Applied Crystallography*, vol. 56, pp. 349–360, 2 2023.

[26] A. J. Schwartz, M. Kumar, B. L. Adams, and D. P. Field, *Electron backscatter diffraction in materials science*. Springer US, 2009.

[27] Y. Kainuma, "The Theory of Kikuchi patterns," *Acta Crystallographica*, vol. 8, pp. 247–257, 5 1955.

[28] Z. Cho, "Tomography," *Encyclopedia of Physical Science and Technology*, pp. 843–877, 1 2003.

Scientific publications

Author contributions

Paper I: Surface grain orientation mapping using grazing incidence X-ray diffraction
Hanna Sjö, A. Shabalin, U. Lienert, J. Hektor, A. Schaefer, P.-A. Carlsson, C. Alwmark, J. Gustafson

I planned the experiment together with Gustafson and performed the data analysis which was developed with the support of Shabalin. I prepared the manuscript and figures.

Paper II: Tomographic surface X-ray diffraction - A method for studying polycrystalline surfaces

I planned the experiment together with Gustafson and performed the data analysis. I prepared the manuscript and figures.